Chemical Engineering Journal 222 (2013) 142–149

Contents lists available at SciVerse ScienceDirect

Chemical Engineering Journal

journal homepage: www.elsevier.com/locate/cej

Ni-catalysts supported on $Zn_xMg_{1-x}Al_2O_4$ for ethanol steam reforming: Influence of the substitution for Mg on catalytic activity and stability

Mariana N. Barroso, Agustin E. Galetti, Manuel F. Gomez, Luis A. Arrúa, Maria C. Abello *

Instituto de Investigaciones en Tecnología Química (INTEQUI-CONICET-UNSL), Chacabuco y Pedernera, 5700 San Luis, Argentina

HIGHLIGHTS

- The Zn substitution for Mg decreased the Ni^{2+} reducibility.
- The Zn substitution for Mg increased basicity and Ni dispersion.
- The strong metal-support interaction and the small Ni particles were crucial in ESR.
- $Ni/MgAl_2O_4$ was the most active catalyst.
- $Ni/MgAl_2O_4$ showed deactivation by graphitic carbon deposition.

GRAPHICAL ABSTRACT

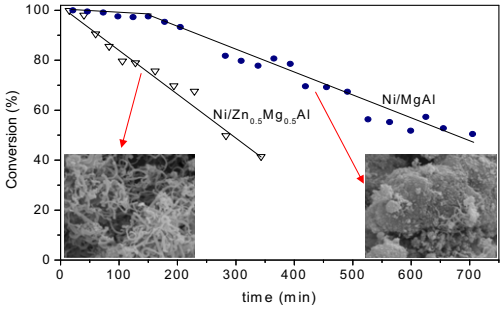

ARTICLE INFO

Article history:
Received 10 October 2012
Received in revised form 5 February 2013
Accepted 18 February 2013
Available online 24 February 2013

Keywords:
$Ni/Zn_xMg_{1-x}Al_2O_4$ catalysts
Hydrogen production
Ethanol reforming

ABSTRACT

Ni catalysts supported on $Zn_xMg_{1-x}Al_2O_4$ spinel oxide have been prepared by the wet impregnation method with 8 wt.% Ni. The samples were characterized by XRD, BET area, TPR, CO_2–TPD, SEM–EDX and TPO and tested in the ethanol steam reforming reaction.

The XRD patterns of Ni catalysts supported on $Zn_xMg_{1-x}Al_2O_4$ with $x = 1$ or 0.5 revealed a highly crystalline spinel phase ($ZnAl_2O_4$ type) and different size particles of NiO. $MgAl_2O_4$ with a poorer crystallinity and NiO were observed for the catalyst supported with $x = 0$. The presence of Mg into the support composition decreased the Ni^{2+} reducibility and increased the basicity and the specific surface area, allowing a high dispersion of metallic particles and an improved resistance to carbon deposition in the ethanol steam reforming reaction. Under the experimental conditions used in this work, $Ni/MgAl_2O_4$ was the most active catalyst but showed deactivation by graphitic carbon deposition.

1. Introduction

The increasing energy demand, the shortage of fossil fuels, the increase in the price of oil and the serious environmental problems have led to the search of effective alternatives to produce hydrogen. The ethanol steam reforming (ESR) reaction provides an interesting method to produce hydrogen from renewable resources [1–4]. This alcohol has a relatively high hydrogen content and its reaction with water is able to produce 6 mol of H_2 per mole of reacted ethanol. Another important advantage is that produced CO_2 could be consumed by biomass growth offering an almost closed carbon cycle. The catalyst for this reaction plays a crucial role and should be active, selective and highly stable. Rh and Ni are so far the best and the most commonly used catalysts [5–9]. However, the limited availability of noble metal makes necessary to develop less expensive catalysts based on non precious metals. Ni catalysts have shown to be very attractive due to the high C–C bond breaking activity and the relatively low cost compared with noble metals [10–18]. The main problem for most of the Ni catalysts is the high deactivation rate related to the formation of carbonaceous deposits and the sintering of metallic particles. The deactivation can occur by covering the active phase due to encapsulating carbon and also by filamentous carbon formation.

The support significantly affects the activity, the selectivity and the long-term stability. They should be resistant to the high tem-

* Corresponding author. Tel./fax: +54 266 4426711.
E-mail address: cabello@unsl.edu.ar (M.C. Abello).

1385-8947/$ - see front matter © 2013 Elsevier B.V. All rights reserved.
http://dx.doi.org/10.1016/j.cej.2013.02.051

peratures attained during the ethanol steam reforming, and they should also be able to maintain the metallic dispersion as high as possible during reaction. Spinel-like oxides (AB_2O_4) have been proposed as catalytic supports due to the low acidity and resistance to coking and sintering [19,20]. In a previous work, the use of NiZnAl catalysts with different Ni loadings showed good performances in ESR, in particular under soft operation conditions (ethanol inlet concentration = 3%, feed molar ratio H_2O:C_2H_5OH = 3.8, reaction temperature = 500–600 °C and catalyst weight = 300 mg) [15]. Guo et al. have claimed that the use of Ni/$MgAl_2O_4$ during the dry reforming of methane [21] allows to attain higher activity and better stability than using Ni/γ-Al_2O_3. Auprete et al. [22] have also obtained an improved deactivation resistance using catalysts supported over $MgAl_2O_4$. Taking into account previous results, the preparation, characterization and activity in ethanol steam reforming over Ni catalysts supported on $Zn_xMg_{x-1}Al_2O_4$ mixed spinel type are presented in this work.

2. Experimental

2.1. Catalyst preparation

The spinel-like oxide $ZnAl_2O_4$ used as support was prepared by the citrate method. Citric acid was added to an aqueous solution that contained the stoichiometric quantities of $Al(NO_3)_3{\cdot}9H_2O$ and $Zn(NO_3)_2{\cdot}6H_2O$. An equivalent of acid per total equivalent of metals was used. The solution was stirred for 10 min and held at boiling temperature for 30 min. Then the solution was concentrated by evaporation under vacuum in a rotavapor at 75 °C until a viscous liquid was obtained. Finally, the dehydration was completed by drying the sample in a vacuum oven at 100 °C for 16 h. The sample was calcined in a 100 mL min^{-1} flow under the following program: at 500 °C in N_2 flow for 2 h, at 700 °C in O_2 (10%)/N_2 flow for 2 h and finally in air at 700 °C for 2 h to remove the carbonaceous residues from citrate chains. The sample was denoted as ZnAl.

The $Zn_xMg_{1-x}Al_2O_4$ mixed supports were prepared by the same procedure using the necessary amounts of $Mg(NO_3)_2{\cdot}6H_2O$ to obtain a partial (x = 0.5) or whole (x = 1) substitution of Zn. These supports were labeled as $Zn_{0.5}Mg_{0.5}Al$ and MgAl, respectively.

Supported Ni catalysts were prepared by wet impregnation using an aqueous solution of $Ni(CH_3COO)_2{\cdot}4H_2O$ (Aldrich, 98%). The nominal composition of Ni was 8 wt.%. After impregnation, the solid was dried at 100 °C overnight and finally they were calcined in air at 600 °C for 3 h.

2.2. Catalyst characterization

All samples were characterized using different physico-chemical methods.

2.2.1. BET surface area

BET surface areas were measured by using a Micromeritics Gemini V analyzer by adsorption of nitrogen at −196 °C on 100 mg of a sample previously degassed at 250 °C for 16 h under flowing N_2.

2.2.2. X-ray diffraction (XRD)

Diffraction patterns were obtained with a RIGAKU diffractometer operated at 30 kV and 20 mA by using Ni-filtered Cu Kα radiation (λ = 0.15418 nm) at a rate of 3° min^{-1} from 2θ = 10° to 90°. The powdered samples were analyzed without a previous treatment after deposition on a quartz sample holder. The identification of crystalline phases was made by matching with the JCPDS files.

2.2.3. Thermal gravimetry (TG–TPO)

The analyses were recorded using DTG-60 Shimadzu equipment. The samples, ca. 15 mg, were placed in a Pt cell and heated from room temperature to 900 °C at a heating rate of 10 °C min^{-1} with an air flow of 50 mL min^{-1}.

2.2.4. Temperature programmed reduction (TPR)

Studies were performed in a conventional TPR equipment. This apparatus consists of a gas handling system with mass flow controllers, a tubular reactor, a linear temperature programmer, a PC for data retrieval, a furnace and various cold traps. Before each run the samples were oxidized in a 50 mL min^{-1} flow of 20 vol.% O_2 in He at 300 °C for 30 min. After that helium was admitted to remove oxygen and finally, the system was cooled to 25 °C. The samples were subsequently contacted with a 50 mL min^{-1} flow of 5 vol.% H_2 in N_2, heated at a rate of 5 °C min^{-1}, from 25 °C to a final temperature of 700 °C and held at 700 °C for 1 h. Hydrogen consumption was monitored by a thermal conductivity detector after removing the formed water. The peak areas were calibrated with H_2 (5 vol.%)/N_2 mixture injections.

2.2.5. Basicity properties

Basicity measurements were determined by CO_2 temperature-programmed desorption, CO_2–TPD, using a conventional flow system with a thermal conductivity detector. 0.2 g was used in each experiment. All samples were prereduced under a (5%)H_2/N_2 flow at 650 °C for 1 h to simulate the catalyst state under reforming conditions. After cooling down to room temperature, the adsorption step started. This step was carried out in pure CO_2 flow for 45 min. Then, the samples were swept with helium for 30 min and finally, the desorption step was performed from room temperature to 700 °C at a heating rate of 10 °C min^{-1} and 30 mL min^{-1} of helium flow. Continuous voltages from the detector cell and reactor thermocouple were converted to digital signals, amplified with a data acquisition workstation and stored in a PC. The total integrated area of the CO_2 band was considered as a measure of total basicity. CO_2 uptake expressed as μmoles CO_2 per g_{cat} and the basic site density expressed as μmoles CO_2 per m^2 were estimated after CO_2 calibration. Three types of basic sites were considered and they were characterized as low, moderate and high-strength. Deconvolution of the desorption curves was achieved taking into account the contribution of each of these sites to the overall desorption curve using Gaussian peaks.

2.2.6. Scanning electron microscopy and energy dispersive X-ray spectroscopy (SEM–EDX)

Scanning electron micrographs were obtained in a LEO 1450 VP. This instrument, equipped with an energy dispersive X-ray microanalyzer (EDAX Genesis 2000) and a Si(Li) detector allowed the analytical electron microscopy measurements. The samples were sputter coated with gold.

2.3. Catalytic test

The ethanol steam reforming reaction was carried out in a stainless steel tubular reactor with an internal diameter of 4 mm operated at atmospheric pressure. The reactor was placed in a vertical furnace with temperature control. The reaction temperature was measured with a coaxial K thermocouple placed inside the sample. The feed to the reactor was a gas mixture of ethanol, water and helium (99.999% research grade). The liquid mixture of ethanol–water was fed at 0.15 mL min^{-1} to an evaporator (operated at 130 °C) through an isocratic pump. The gas stream flow rates were controlled by mass flowmeters. The experimental set-up has a low pressure proportional relief valve for early detection of catalytic bed plugging. The molar ratio in the feed was H_2O:C_2H_5OH = 4.8

Table 1
Some properties of $Ni/Zn_xMg_{1-x}Al_2O_4$ catalysts.

Sample	S_{BET} (m^2g^{-1})	d_{NiO}^{XRD} [b] (nm)	d_{Ni}^{XRD} [b] (nm)	
			Reduced	Used
Ni/ZnAl	27 (40)[a]	26.0	29.3	n.d
$Ni/Zn_{0.5}Mg_{0.5}Al$	41 (76)	18.4	17.2	25.6
Ni/MgAl	138 (170)	≈5	8.3	18.6

[a] Values between brackets correspond to bare supports.
[b] Calculations are based on the line broadening of the NiO (200) and Ni^0 (200) diffraction lines.

being the ethanol flow 1.02×10^{-3} mol min^{-1}. The molar ratio was near to the optimum one suggested from a study of the energy integration and the maximum efficiency in an ethanol processor for hydrogen production and a fuel cell [23,24]. The catalyst weight was 50 mg (0.3–0.4 mm particle size range) diluted with 276 mg of an inert material (quartz grinded in the same particle size). The catalyst was heated to reaction temperature under a He flow, then the mixture with $C_2H_5OH + H_2O$ was allowed to enter into the reactor to carry out the catalytic test. The reactants and reaction products were analyzed *on-line* by gas chromatography. H_2, CH_4, CO_2 and H_2O were separated by a 1.8 m Carbosphere (80–100 mesh) column and analyzed by a TC detector. Nitrogen was used as an internal standard. Besides, CO was analyzed by a flame ionization detector after passing through a methanizer. Higher hydrocarbons and oxygenated products (C_2H_4O, $C_2H_4 + C_2H_6$, C_3H_6O, C_2H_5OH, etc.) were separated in Rt-U PLOT capillary column and analyzed with FID using N_2 as carrier gas. The homogeneous contribution was tested with the empty reactor. These runs showed an ethanol conversion lower than 5% at 650 °C.

Ethanol conversion (X_{EtOH}), selectivity to carbon products (S_i) and hydrogen yield (Y_{H2}) were estimated as

$$X_{EtOH} = \frac{F_{EtOH}^{in} - F_{EtOH}^{out}}{F_{EtOH}^{in}} \times 100$$

$$S_i = \frac{v_i F_i^{out}}{2(F_{EtOH}^{in} - F_{EtOH}^{out})} \times 100$$

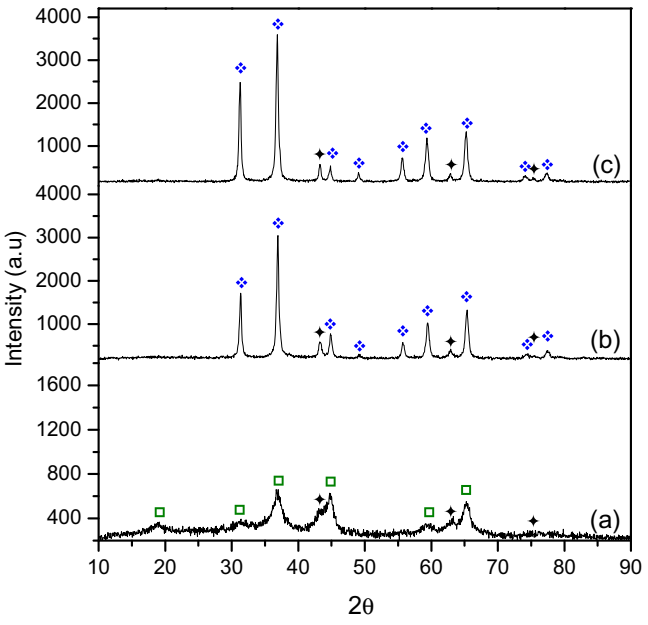

Fig. 1. X-ray diffraction patterns of fresh (a) Ni/MgAl; (b) $Ni/Zn_{0.5}Mg_{0.5}Al$ and (c) Ni/ZnAl catalysts. ❖: $ZnAl_2O_4$, □: $MgAl_2O_4$ and ✦: NiO.

$$Y_{H_2} = \frac{F_{H_2}^{out}}{F_{EtOH}^{in}}$$

F_i^{in} and F_i^{out} are the molar flow rates of product "*i*" at the inlet and outlet of the reactor, respectively, and v_i is the number of carbon atoms in "*i*".

3. Results and discussion

Table 1 summarizes some characteristics of fresh catalysts. The specific surface values for the supports vary from 170 m^2/g for MgAl (0% Zn) to 40 m^2/g for ZnAl (0% Mg). The S_{BET} increases with the Zn substitution in agreement with other results reported in literature [25]. The ZnAl and $Zn_{0.5}Mg_{0.5}Al$ supports present values compatible with the high calcination temperature and the crystallinity degree observed by X-ray diffraction. The MgAl support shows a high specific surface in spite of the calcination at 700 °C for 4 h. Guo et al. [26] have reported specific surface values between 197 and 182 m^2/g for $MgAl_2O_4$ prepared by sol–gel method and calcined at 700 and 800 °C, respectively. The Ni impregnation decreases the S_{BET} being the highest decreasing over $Ni/Zn_{0.5}Mg_{0.5}$-Al sample (47%). A high specific surface area is observed for Ni/MgAl catalyst. Guo et al. have also reported lower specific surface values (80 and 78 m^2/g) for $Ni/MgAl_2O_4$ with 5 and 10 wt.% Ni [21]. In all the cases type IV adsorption–desorption isotherms are obtained with H1 hysteresis which are characteristics of systems with cylindrical pores.

X-ray diffraction pattern for the fresh Ni/MgAl sample shown in Fig. 1a reveals the reflexion lines which could be unequivocally assigned to $MgAl_2O_4$ (2θ = 19.03°, 31.3°, 36.8°, 44,8°, 59.4° and 65.2°, JCPDS-21-1152). The low intensity of reflexion lines and the broadened peaks indicate a low crystallinity for $MgAl_2O_4$. A higher calcination temperature should be necessary to reach a better crystallization degree [21,26–28]. Lines assigned to NiO (2θ = 43.3°, 37.3° and 62.9°, JCPDS-4-835) are also observed, which broadenings suggest that NiO particles on Ni/MgAl are smaller in size than those on Ni/Zn0.5Mg0.5Al and Ni/ZnAl. For the Ni/ZnAl sample, Fig. 1c, the characteristic symmetric and intense reflexion lines of the $ZnAl_2O_4$ spinel (2θ = 31.3°, 36.9°, 44.8°, 59.4° and 65.3°, JCPDS-5-669) are clearly detected indicating a high crystalline order. The reflexion lines of NiO are also more intense than for Ni/MgAl. For $Ni/Zn_{0.5}Mg_{0.5}Al$ sample, Fig. 1b, the diffraction pattern resembles to that of Ni/ZnAl. The ionic radius of Zn^{2+} (0.74 Å) and Mg^{2+} (0.65 Å) are similar, therefore, the substitution for Mg does not disturb the spinel structure. The formation of $MgAl_2O_4$ which main reflexion lines are coincident with those of $ZnAl_2O_4$, MgO and Al_2O_3 could not be ruled in $Ni/Zn_{0.5}Mg_{0.5}Al$ sample. The particle size of NiO, d_{NiO}^{XRD}, estimated by Scherrer follows the order of Ni/ZnAl > $Ni/Zn_{0.5}Mg_{0.5}Al \gg$ Ni/MgAl, Table 1. The small particle size on Ni/MgAl is a consequence of the highest specific surface area and also of the strong interaction reached between NiO and MgAl support (shown further).

The reduction profiles from TPR, illustrated in Fig. 2, reveal that the support composition has a significant effect on the Ni reducibility. The TPR for Ni/MgAl sample shows a H_2 consumption between 450 and 700 °C, with a maximum at ≈670 °C. This peak can be attributed to the reduction of Ni^{+2} species from small NiO particles which are well dispersed and strongly interacting with the Mg aluminate matrix. There is a shoulder at 580 °C that could indicate the presence of a Ni^{2+} fraction with a lower interaction with the support. Similar results were reported for $Ni/MgO–Al_2O_3$ catalysts calcined at 650 °C [11]. Corthals et al. have also reported one reduction peak between 700 and 1000 °C, for Ni(10 wt.%)/$MgAl_2O_4$ [29]. The XRD of the reduced sample (after TPR experiments), Fig. 3a, reveals the absence of NiO and the presence of

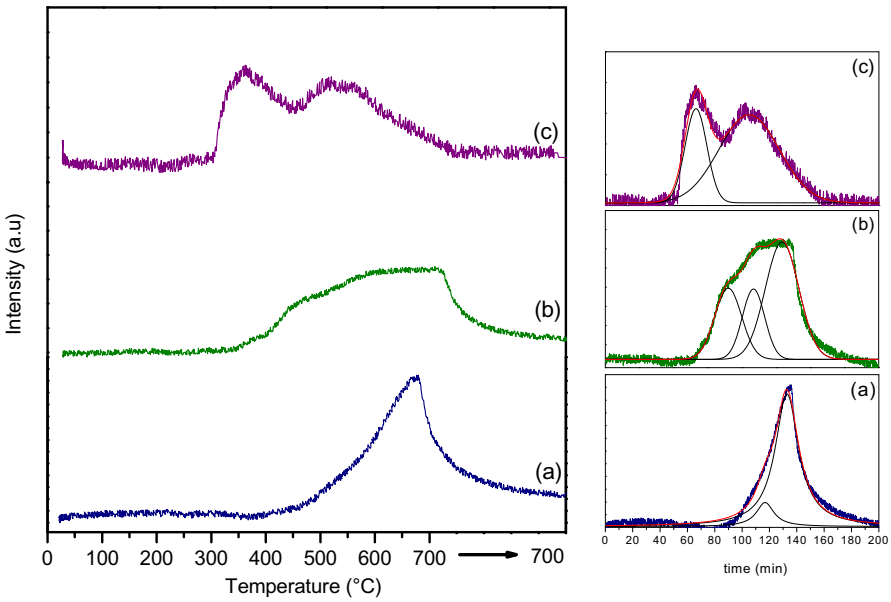

Fig. 2. Temperature programmed reduction profiles for (a) Ni/MgAl; (b) Ni/$Zn_{0.5}Mg_{0.5}$Al and (c) Ni/ZnAl catalysts.

weak lines corresponding to Ni^0. For Ni/$Zn_{0.5}Mg_{0.5}$Al, a complex TPR profile with at least three overlapped peaks is obtained, Fig. 2b. The broad band of H_2 consumption between 350 and 700 °C could be attributed to the reduction of Ni^{2+} to Ni^0 in different environments. The XRD, Fig. 3b, shows the diffraction lines corresponding to the spinel and Ni^0. The low intensities of reflexion lines are due to the small amount of powder used into the glass XRD sample holder. Finally, the TPR profile for Ni/ZnAl sample reveals two peaks at 355° and 518 °C. The first one is assigned to the reduction of Ni^{2+} species weakly interacted with the support and the second one to the reduction of Ni^{2+} species more strongly interacted with $ZnAl_2O_4$. The diffraction pattern of reduced sample, Fig. 3c, shows the presence of Ni^0 and the peaks assigned to $ZnAl_2O_4$ which are not practically altered by reduction. A correlation between the reducibility of nickel, the particle sizes and the metal-support interaction can be inferred. Larger NiO particles, weakly or moderately interacted with the support, lead to an improved NiO reducibility. Pure NiO reduces at 364 °C under the same reduction conditions [15]. The particle size of Ni^0, d_{Ni}^{XRD}, estimated by Scherrer follows the order of Ni/ZnAl > Ni/$Zn_{0.5}Mg_{0.5}$Al ≫ Ni/MgAl, Table 1. A summary of TPR results is shown in Table 2. The hydrogen consumption is estimated by the integration of the H_2–TPR profile and the extent of reduction is lower for Ni/MgAl. The abundance of different Ni^{2+} species at low, medium and high temperature is obtained by deconvolution of TPR profiles. The Ni^{2+} species strongly interacted with the support increases from 53% for Ni/$Zn_{0.5}Mg_{0.5}$Al to 88.2% for Ni/MgAl, but they are absent in Ni/ZnAl sample. The Ni^{2+} reducibility decreases by the presence of Mg but the metal-support interactions increases.

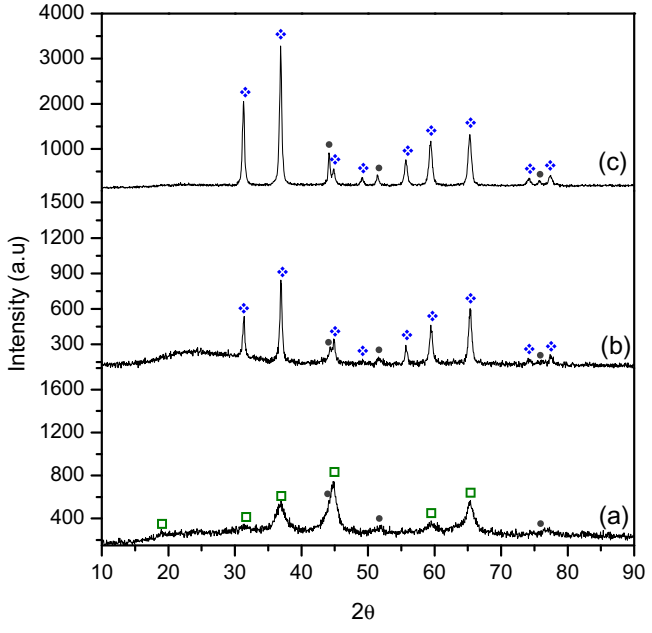

Fig. 3. X-ray diffraction patterns of reduced (a) Ni/MgAl; (b) Ni/$Zn_{0.5}Mg_{0.5}$Al and (c) Ni/ZnAl catalysts. ❖: $ZnAl_2O_4$, □: $MgAl_2O_4$ and ●: Ni^0.

Basic properties were investigated using the adsorption of probe molecules by TPD. CO_2–TPD profiles for the catalysts are illustrated in Fig. 4. The profiles for Ni/ZnAl and Ni/$Zn_{0.5}Mg_{0.5}$Al have a similar shape and they are characterized by a broad asymmetric desorption pattern, spanning the range 25–700 °C, with maxima at 90° and 130 °C, respectively. In comparison with the sample without Zn, the basicity is markedly lower on Ni/ZnAl and Ni/$Zn_{0.5}Mg_{0.5}$Al samples. The profile for Ni/MgAl presents an intense peak at low temperature around 100 °C and a second one between 170° and 240° suggesting the presence of basic sites with a moderate strength. The shape of CO_2–TPD profiles reveals a considerable heterogenity in the basic site strength distribution. Bezen et al. [25] have reported the acid–base properties of Zn–Mg–Al mixed oxides prepared by coprecipitation method. They studied the effect to vary the Zn^{2+}/Mg^{2+} ratio from 0.33 to 3 keeping the amount of Al^{3+} constant. Their CO_2–TPD profiles were very similar in shape and in the maximum temperatures to those showed in Fig. 4. Di Cosimo et al. [30] have reported three desorption bands reaching maximum desorption rates at 100, 170 and 270 °C for Mg–Al mixed oxides obtained from hydrotalcite precursors. These three species of adsorbed CO_2 correspond to three different types of surface basic sites (indentified by IR) that were characterized as low (bicarbonate), moderate (bidentate carbonate) and high strength (unidentate carbonate). The total basicity and density obtained by the integration of TPD curves are reported in Table 3. The total basicity values expressed as μmoles CO_2 g_{cat}^{-1} follow the se-

Table 2
Results of temperature programmed reduction.

Sample	H_2/Ni (mol/mol)	T_L (°C)	T_M (°C)	T_H (°C)	Ni^{2+} distribution (%)		
					L	M	H
Ni/ZnAl	0.91	355	518	–	27.9	72.1	–
$Ni/Zn_{0.5}Mg_{0.5}Al$	1.00	444.5	540	647	25.8	21.2	53.0
Ni/MgAl	0.85	–	580	668	–	11.8	88.2

Contribution of Ni^{2+}species at L: low temperature, M: medium temperature, H: high temperature determined by deconvolution of TPR profiles

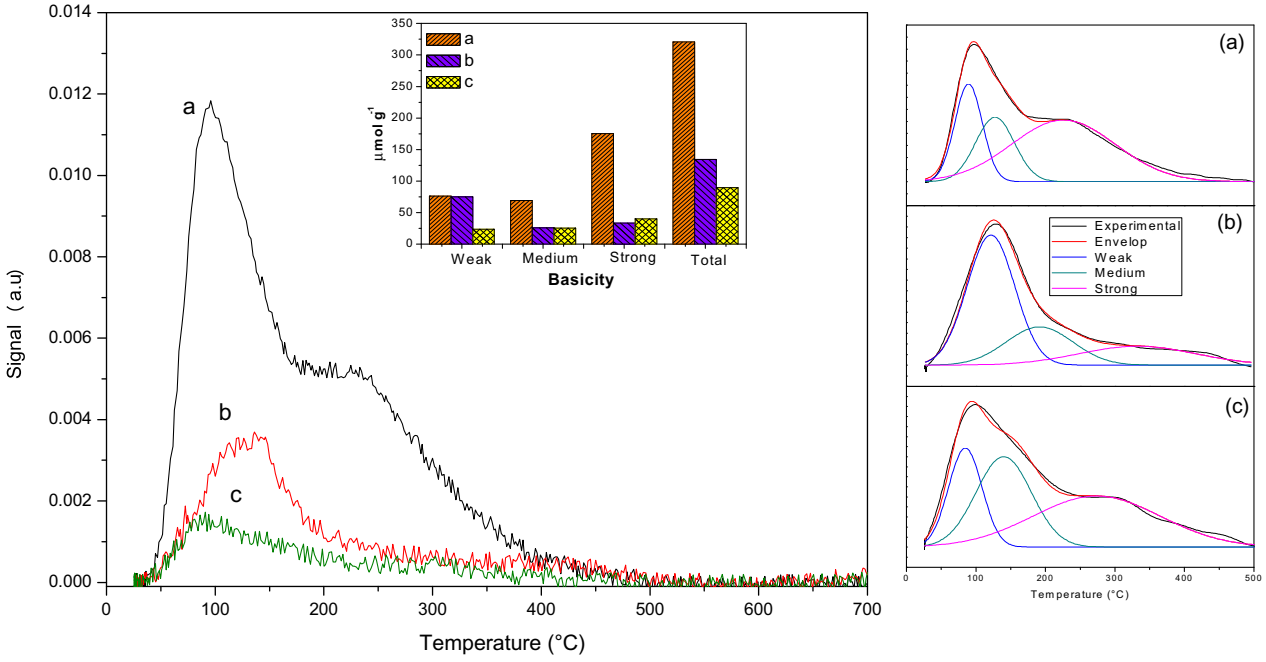

Fig. 4. CO_2–TPD profiles for reduced (a) Ni/MgAl; (b) $Ni/Zn_{0.5}Mg_{0.5}Al$ and (c) Ni/ZnAl catalysts.

quence: Ni/MgAl > $Ni/Zn_{0.5}Mg_{0.5}Al$ > Ni/ZnAl. However, the basic site density expressed as μmoles CO_2 per m^2 shows an inverse order. The relative contribution of each desorption peak is estimated by deconvolution of CO_2 profiles, and the values are also shown in the insert of Fig. 4 and Table 3. The abundance of weak and moderate sites decreases from 26.5 and 28.5 on Ni/ZnAl to 23.8 and 21.5 on Ni/MgAl, respectively, and the abundance of strong basic sites increases from 44.9% on Ni/ZnAl to 54.6% on Ni/MgAl. Rossi et al. [31] have reported a strong parallelism in the basic sites distribution on the stoichiometric spinels $MgAl_2O_4$ and $ZnAl_2O_4$ and surprisingly, very similar to that of alumina. The observed differences could be attributed to a partial inversion of the spinel structure which could be present at the surface exposing both the bivalent ions and the trivalent ion (Al^{3+}), and thus increasing the basicity. The $Ni/Zn_{0.5}Mg_{0.5}Al$ sample shows the highest abundance of weak basic sites.

Table 3
Basic properties of reduced catalysts by CO_2-TPD.

Sample	Basicity μmol CO_2 (m^{-2})	Basic site distribution (%)		
		W	M	S
Ni/ZnAl	3.4 (89.7)[a]	26.5	28.5	44.9
$Ni/Zn_{0.5}Mg_{0.5}Al$	3.3 (134.5)	55.7	19.3	24.9
Ni/MgAl	2.3 (320.5)	23.8	21.5	54.6

W: weak, M: moderate, S: strong basicity
[a] Values between brackets correspond to basicity expressed as μmol CO_2 g_{cat}^{-1}.

The overall performance of the catalysts studied during ethanol steam reforming is evaluated in terms of ethanol conversion, product distribution and stability. The experimental run for Ni/ZnAl catalyst was interrupted after few minutes in reaction due to the severe increase of the reactor pressure bed.

The evolution of ethanol conversion along the time on stream at 650 °C, without a previous reduction for Ni/MgAl and $Ni/Zn_{0.5}Mg_{0.5}Al$ is shown in Fig. 5. A high initial ethanol conversion and a significant conversion decay are observed for both catalysts.

On Ni/MgAl catalyst the initial conversion is around 100% and is kept constant until 100 min, afterward the activity significantly decays reaching a conversion of 50.5% at 700 min in time on stream. The product distribution for this catalyst is shown in Fig. 6a. The main products obtained are H_2, CO_2 and CO. Minor amounts of C_2H_4O and CH_4 are also produced. The decrease in conversion is accompanied by a decrease in H_2 and CO_2 selectivities and by an increase in C_2H_4O selectivity [17]. The selectivities to CO and CH_4 are almost constant during the reaction time (28.5% and 7.5%, respectively). The H_2 yield decreases from 4.8 to 3 mol H_2/mol C_2H_5OH. Other products such as ethylene, acetone and propylene are also obtained with selectivities lower than 2%.

On the $Ni/Zn_{0.5}Mg_{0.5}Al$ sample the ethanol conversion decreases from 100% to 41.5% after 340 min in time on stream. This experimental run was also interrupted at this time due to the severe increase of the reactor pressure bed. The product distribution for this catalyst is shown in Fig. 6b. From the beginning of reaction, the decrease in conversion is accompanied by a fast decrease in H_2, CO_2 and CO and by an important increase in C_2H_4O. The steam reform-

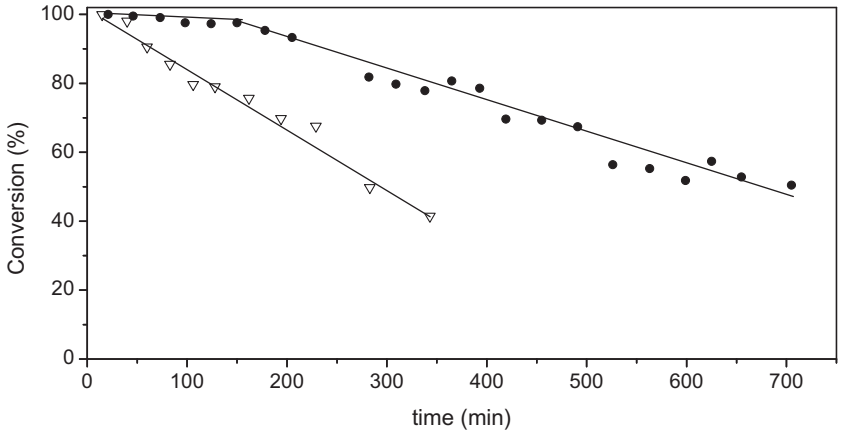

Fig. 5. Ethanol conversion as a function of reaction time on stream. ▽ $Ni/Zn_{0.5}Mg_{0.5}Al$, and ● Ni/MgAl. Reaction temperature: 650 °C, molar ratio $H_2O/C_2H_5OH = 4.9$.

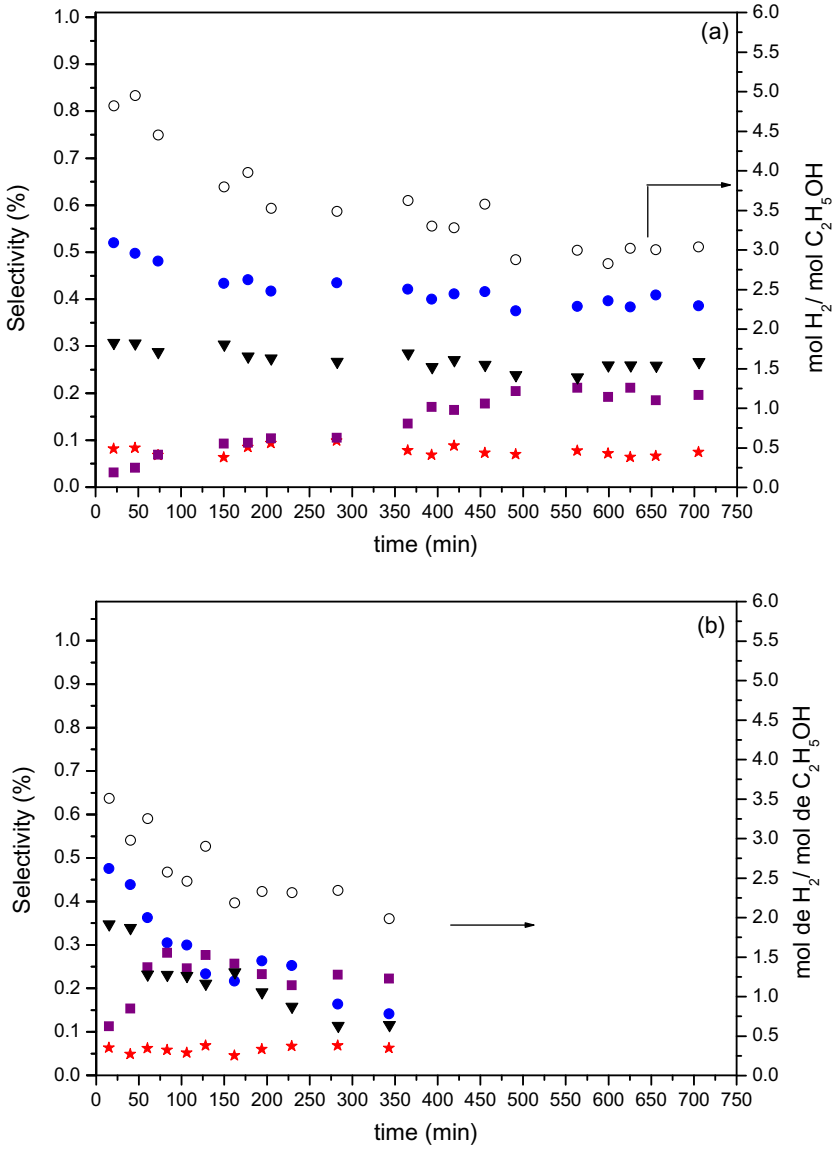

Fig. 6. Product distribution in the ethanol steam reforming reaction over (a) Ni/MgAl and (b) $Ni/Zn_{0.5}Mg_{0.5}Al$ at 650 °C and atmospheric pressure. ○: mol H_2/mol C_2H_5OH, ■: C_2H_4O, ★: CH_4, ●: CO_2, and ▼: CO.

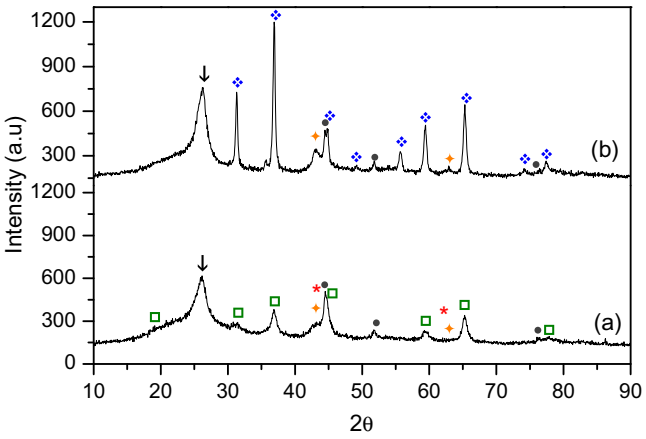

Fig. 7. X-ray diffraction patterns of used (a) Ni/MgAl and (b) $Ni/Zn_{0.5}Mg_{0.5}Al$. catalysts after ethanol steam reforming reaction ❖: $ZnAl_2O_4$, □: $MgAl_2O_4$, ✱: MgO, ✦: NiO, ●: Ni^0 and ↓: C.

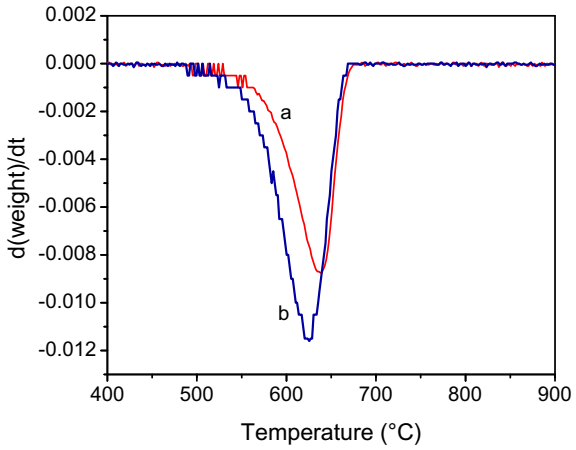

Fig. 8. Derivative TGA of used (a) Ni/MgAl; and (b) $Ni/Zn_{0.5}Mg_{0.5}Al$ catalysts carried out under air flow .

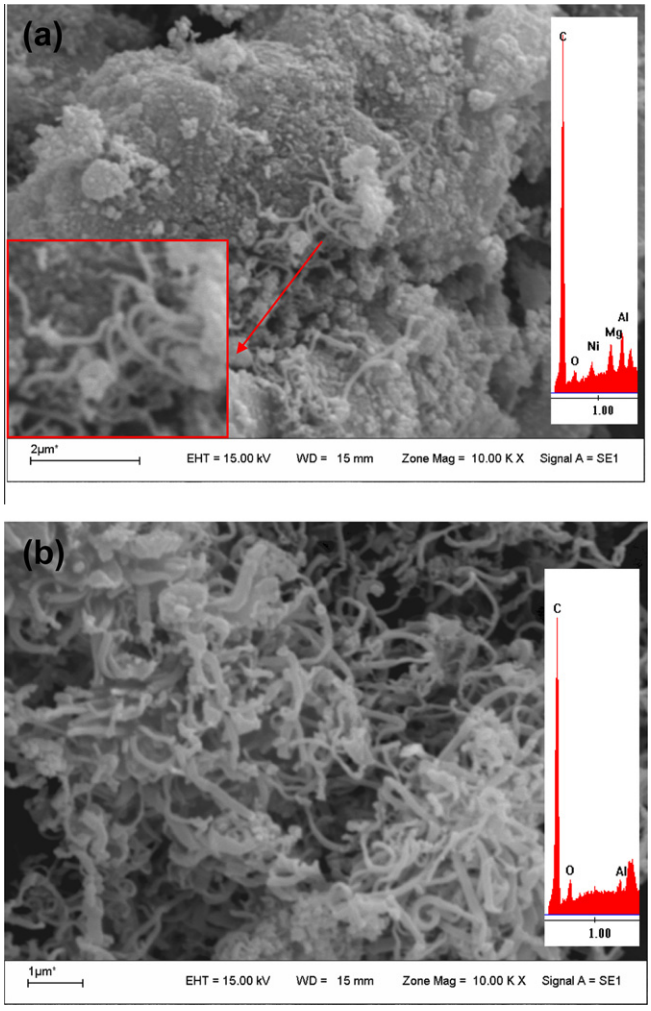

Fig. 9. SEM images of used (a) Ni/MgAl and (b) $Ni/Zn_{0.5}Mg_{0.5}Al$ catalysts.

ing reaction is quickly suppressed and the dehydrogenation appears as a predominant reaction.

The XRD patterns of used samples are shown in Fig. 7a and b. $MgAl_2O_4$ and Ni^0 are observed on Ni/MgAl. The experimental tests are carried out without a previous reduction of catalyst. XRD patterns of used catalysts reveal that Ni^{+2} species have been reduced to Ni^0 under the reforming environment as expected. Weak peaks are detected at $2\theta = 43°$ and 62.5°. They could be attributed to the presence of unreduced NiO and/or MgO ($2\theta = 36.9°$, 42.9°, 62.3°, 78.6° JCPDS-4-829) that could be segregated or expelled from the aluminate matrix. Besides, a broad peak corresponding to graphitic carbon at $2\theta = 26.4°$ (JCPDS-41-1487) is clearly detected. For the $Ni/Zn_{0.5}Mg_{0.5}Al$ sample the characteristic lines of spinel, Ni^0 and an intense diffraction peak corresponding to graphitic carbon are also observed. NiO and MgO could also be present. The particle size of Ni^0, d_{Ni}^{XRD}, estimated by Scherrer and shown in Table 1, indicates a sintering of metallic particle under reforming conditions.

The carbon amounts for used samples quantified by TG–TPO are shown in Fig. 8. For Ni/MgAl the most important weight loss is at 625 °C whereas for $Ni/Zn_{0.5}Mg_{0.5}Al$ is at 638 °C. They are attributed to the combustion of graphitic carbon (graphitic filamentous carbon or polymorphic forms of graphite) in agreement with the XRD results and data from literature [21,32]. The amounts of coke are 2.97 and 2.82 gC g_{cat}^{-1} for Ni/MgAl (reaction time 700 min) and $Ni/Zn_{0.5}Mg_{0.5}Al$ (reaction time 340 min), respectively. The carbonaceous species could be deposited on metallic particles explaining the strong deactivation and also on the aluminate matrix. In the case of $Ni/Zn_{0.5}Mg_{0.5}Al$, the reactor plugging occurs in less than 6 h due to the large amount of coke formed which is favorably formed by the high metallic particle size and the lower strong basicity of the support. Sanchez-Sanchez et al. [11] have also reported an important amount of carbon on $Ni/MgO–Al_2O_3$ catalysts when they were tested in ethanol steam reforming at 500 °C during 1440 min (molar ratio $H_2O/EtOH = 3.0$ and GHSV = 24 487 h^{-1}).

The formation of carbonaceous deposits on used catalysts is also evidenced by SEM. The SEM micrograph for the Ni/MgAl sample, Fig. 9a, shows a lower amount of carbon filaments with smaller diameters than those observed for $Ni/Zn_{0.5}Mg_{0.5}Al$, Fig. 9b. Besides, the EDX analysis shows that the carbon coverage avoids the Ni detection on $Ni/Zn_{0.5}Mg_{0.5}Al$. On this sample an important fraction of Ni surface is blocked with carbon filaments or polymorphic forms of graphite that should be responsible for the discontinuation of the catalytic test.

The strong metal-support interaction and the small particle size of Ni seem to play a crucial role more than the basicity of the support. The Ni/ZnAl and Ni/MgAl catalysts show a similar basic sites distribution. The 72% of Ni^{2+} species interacts in a moderate way with the support on Ni/ZnAl, whereas near to 90% of Ni^{2+} strongly interacts on Ni/MgAl. The $Ni/Zn_{0.5}Mg_{0.5}Al$ catalyst shows the lowest strong basicity which is compensated with the presence of 53% of Ni^{2+}strongly interacted with the support.

4. Conclusions

Ni catalysts supported on $Zn_xMg_{1-x}Al_2O_4$ with 8 wt.% Ni were prepared by the wet impregnation method, characterized by different techniques and tested in ethanol steam reforming to produce hydrogen.

The presence of Mg in the spinel composition increased the specific surface area, the interaction of Ni^{2+} with the aluminate matrix and the basicity expressed as μmol CO_2 g_{cat}^{-1}. Besides, it showed an improved metallic dispersion of nickel and a higher resistence of carbon deposition. However, the amount of carbonaceous deposits and the deactivation rate under reforming conditions were important. $Ni/MgAl_2O_4$ was the most active and stable catalyst under the mild experimental conditions used in this work

Acknowledgments

Financial supports are acknowledged to CONICET, ANPCyT and Universidad Nacional de San Luis.

References

[1] P.G. Gray, M.I. Petch, Advances with HotSpot™ fuel processing: efficient hydrogen production for use with solid polymer fuel cells, Platinium Met. Rev. 44 (2000) 108–111.
[2] P.D. Vaidya, A.E. Rodrigues, Insigth into steam reforming of ethanol to produce hydrogen for fuel cells, Chem. Eng. J. 117 (2006) 39–49.
[3] A. Carrero, J.A. Calles, A.J. Vizcaíno, Effect of Mg and Ca addition on coke deposition over $Cu–Ni/SiO_2$ catalysts for ethanol steam reforming, Chem. Eng. J. 163 (2010) 395–402.
[4] M. Domínguez, G. Cristiano, E. López, J. Llorca, Ethanol steam reforming over cobalt talc in a plate microreactor, Chem. Eng. J. 176–177 (2011) 280–285.
[5] M. Ni, D. Leung, M.K. H Leung, A review on reforming bio-ethanol for hydrogen production, Int. J. Hydrogen Energy 32 (2007) 3238–3247 (all references therein).
[6] H.-S. Roh, Y. Wang, D. King, Selective production of H_2 from ethanol at low temperatures over $Rh/ZrO_2–CeO_2$ catalysts, Top. Catal. 49 (2008) 32–37.
[7] M. Dömök, A. Oszkó, K. Baan, I. Sarusi, A. Erdöhelyi, Reforming of ethanol on $Pt/Al_2O_3–ZrO_2$ catalyst, Appl. Catal. A 383 (2010) 33–42.
[8] N. Rao Pela, A. Mubayi, D. Kunzru, Steam reforming of ethanol over $Rh/CeO_2/Al_2O_3$ catalysts in a micro channel reactor, Chem. Eng. J. 167 (2011) 578–587.
[9] Göksel Özkan, Serdar Gök, Gülay Özkan, Active carbon-supported Ni, Ni/Cu and Ni/Cu/Pd catalysed steam reforming of ethanol for the production of hydrogen, Chem. Eng. J. 171 (2011) 1270–1275.
[10] Prakash Biswas, Deepak Kunzru, Steam reforming of ethanol for production of hydrogen over Ni/CeO–ZrO catalyst: effect of support and metal loading, Int. J. Hydrogen Energy 32 (2007) 969–980.
[11] M.C. Sánchez-Sánchez, R.M. Navarro, J.L.G. Fierro, Ethanol steam reforming over $Ni/M_xO_y–Al_2O_3$ (M = Ce, La, Zr and Mg) catalysts: influence of support on the hydrogen production, Int. J. Hydrogen Energy 32 (2007) 1462–1471.
[12] F. Frusteri, S. Freni, V. Chiodo, L. Spadaro, O. Di Blasi, G. Bonura, S. Cavallaro, Steam reforming of bio-ethanol on alkali-doped Ni/MgO catalysts: hydrogen production for MC fuel cell, Appl. Catal. A: Gen. 270 (2004) 1–7.
[13] J.W.C. Liberatori, R.U. Ribeiro, D. Zanchet, F.B. Noronha, J.M.C. Bueno, Steam reforming of ethanol on supported nickel catalysts, Appl. Catal. A: Gen. 327 (2007) 197–204.
[14] J. Comas, F. Mariño, M. Laborde, N. Amadeo, Bio-ethanol steam reforming on Ni/Al_2O_3 catalyst, Chem. Eng. J. 98 (2004) 61–68.
[15] M.N. Barroso, M.F. Gomez, L.A. Arrua, M.C. Abello, Hydrogen production by ethanol reforming over NiZnAl catalysts, Appl. Catal. A: Gen. 304 (2006) 116–123.
[16] V. Mas, G. Baronetti, N. Amadeo, M. Laborde, Ethanol steam reforming using Ni(II)–Al(III) layered double hydroxide as catalyst precursor: kinetic study, Chem. Eng. J. 138 (2008) 602–607.
[17] L. Barattini, G. Ramis, C. Resini, G. Busca, M. Sisani, U. Costantino, Reaction path of ethanol and acetic acid steam reforming over Ni–Zn–Al catalysts. Flow reactor studies, Chem. Eng. J. 153 (2009) 43–49.
[18] F. Seyedeyn-Azad, J. Abedi, E. Salehi, T. Harding, Production of hydrogen via steam reforming of bio-oil over Ni-based catalysts: effect of support, Chem. Eng. J. 180 (2012) 145–150.
[19] J. Sehested, J.A.P. Gelten, I.N. Remediakis, H. Bengaard, J.K. Norskov, Sintering of nickel steam-reforming catalysts: effects of temperature and steam and hydrogen pressures, J. Catal. 223 (2004) 432–443.
[20] A.M. Gadalla, B. Bower, The role of catalyst support on the activity of nickel for reforming methane with CO_2, Chem. Eng. Sci. 43 (1988) 3049–3062.
[21] J. Guo, H. Lou, H. Zhao, D. Chai, X. Zheng, Dry reforming of methane over nickel catalysts supported on magnesium aluminate spinels, Appl. Catal. A: Gen. 273 (2004) 75–82.
[22] F. Auprêtre, C. Descorme, D. Duprez, D. Casanave, D. Uzio, Ethanol steam reforming over $Mg_xNi_{1-x}Al_2O_3$ spinel oxide-supported Rh catalysts, J. Catal. 233 (2005) 464–477.
[23] J.A. Francesconi, M.C. Mussati, R.O. Mato, P.A. Aguirre, Analysis of the energy efficiency of an integrated ethanol processor for PEM fuel cell systems, J. Power Sources 167 (2007) 151–161.
[24] A. Perna, Hydrogen from ethanol: theoretical optimization of a PEMFC system integrated with a steam reforming processor, Int. J. Hydrogen Energy 32 (2007) 1811–1819.
[25] M. Bezen, C. Breitkopf, J.A. Lercher, On the acid–base properties of Zn–Mg–Al mixed oxides, Appl. Catal. A: Gen. 399 (2011) 93–99.
[26] J. Guo, H. Lou, H. Zhao, X. Wang, X. Zheng, Novel synthesis of high surface area $MgAl_2O_4$ spinel as catalyst support, Mater. Lett. 58 (2004) 1920–1923.
[27] E.L. Foletto, R.W. Alves, S.L. Jahn, Preparation of Ni/Pt catalysts supported on spinel ($MgAl_2O_4$) for methane reforming, J. Power Sources 161 (2006) 531–534.
[28] H. Zhang, X. Jia, Z. Liu, Z. Li, The low temperature preparation of nanocrystalline $MgAl_2O_4$ spinel by citrate sol–gel process, Mater. Lett. 58 (2004) 1625–1628.
[29] S. Corthals, J. Van Nederkassel, J. Geboers, H. De Winne, J. Van Noyen, B. Moens, B. Sels, P. Jacobs, Influence of composition of $MgAl_2O_4$ supported $NiCeO_2ZrO_2$ catalysts on coke formation and catalyst stability for dry reforming of methane, Catal. Today 138 (2008) 28–32.
[30] J.I. Di Cosimo, V.K. Diez, M. Xu, E. Iglesias, C. Apesteguía, Structure and surface and catalytic properties of Mg–Al basic oxides, J. Catal. 178 (1998) 499–510.
[31] P. Rossi, G. Busca, V. Lorenzelli, M. Waqif, O. Saur, J.-C. Lavalley, Surface basicity of mixed oxides: magnesium and zinc aluminates, Langmuir 7 (1991) 2677–2681.
[32] T.G. Ros, A. Van Dillen, J. Geus, D. Koningsberger, Surface oxidation of carbon nanofibres, Chem. Eur. J. 8 (2002) 1151–1161.